Characterization of distinct Arctic Aerosol Accumulation Modes and their Sources

Lange, R.; Dall'Osto, Manuel; Skov, H.; Nielsen, I.E.; Beddows, David; Simo, R.; Harrison, Roy; Massling, A.

DOI:
10.1016/j.atmosenv.2018.03.060

Characterization of distinct Arctic aerosol accumulation modes and their sources

R. Lange[1]*, M. Dall´Osto[2], H. Skov[1], J. K. Nøjgaard[1], I. E. Nielsen[1], D.C.S. Beddows[3], R. Simo[2], Roy M. Harrison[3†] and A. Massling[1]

[1]*Department of Environmental Science, Aarhus University, Frederiksborgvej 399, 4000, Roskilde, Denmark*

[2]*Institute of Marine Sciences, ICM-CSIC, Passeig Marítim de la Barceloneta, 37-49. E-08003, Barcelona, Spain; *also E-mail: dallosto@icm.csic.es.*

[3]*National Centre for Atmospheric Science, University of Birmingham, Edgbaston, Birmingham, B15 2TT, United Kingdom*

[†]*Also at: Department of Environmental Sciences / Center of Excellence in Environmental Studies, King Abdulaziz University, PO Box 80203, Jeddah, 21589, Saudi Arabia*

*Corresponding author: Robert.lange@envs.au.dk

Keywords

Arctic aerosol, accumulation mode, Arctic haze, biogenic Aerosol, CCN

Highlights

- Accumulation mode aerosol is measured in North East Greenland during a 7 year record, apportioning 56% of total aerosol size distributions.
- Three aerosol categories are found: accumulation *Haze* (32%), accumulation *Aged* (14%) and accumulation *Bimodal* (6%).
- Accumulation categories have very distinct chemical and physical properties across different seasons.
- Arctic accumulation mode aerosols during summer coexist with a smaller Aitken mode, likely biogenic.
- Cloud Condensation Nuclei (CCN) measurements suggest that ultrafine aerosol (~30-60nm) drives CCN concentrations in the Arctic during summer.

Abstract

Measurements of aerosol number size distributions (9-915 nm), as well as aerosol chemistry and cloud condensation nuclei (CCN) activity, were undertaken at Villum Research Station, Station Nord (VRS) in North Greenland during a 7 year record (2010-2016). Clustering analysis on daily size distributions identified several k-means SMPS clusters. K-means clusters of accumulation aerosols (with main size modes >100 nm) accounted for 56% of the total aerosol time sampling period (89-91% during February-April, 1-3% during June-August). By air trajectory association, diurnal variation patterns, and relationship to meteorological and pollution variables, three typical accumulation-mode aerosol categories were identified: *Haze* (32% of the time), *Bimodal* (14%) and *Aged* (6%). In brief: (1) *Haze* accumulation aerosol shows a single mode at 150 nm, peaking in February-April, with highest loadings of sulfate and black carbon concentrations; (2) *Aged* accumulation aerosol shows a single mode at 213 nm, peaking in September-October and is associated with cloudy and humid weather conditions during autumn; and (3) Accumulation *Bimodal* aerosol shows two modes at 38 nm and 150 nm, peaking in June-August, with the highest ratio of organics to sulfate concentrations. The three aerosol categories were considered alongside Cloud Condensation Nuclei (CCN) concentrations. We suggest that organic compounds - likely biogenic in nature and responsible for the smaller mode in the *Bimodal* category - contribute significantly to the CCN activity. It is concluded that - at least during summer - an Aitken mode, biogenic in origin always coexists with an accumulation mode, stressing the importance of better characterizing the marine ecosystem and the aerosol-mediated climate effects in the Arctic.

1. Introduction

The Arctic, one of the most sensitive regions to climate change, is warming at a rate twice as rapid as the global average (AMAP, 2011). Currently, atmospheric aerosols are poorly characterized in Arctic climate models. Aerosol particles may perturb the radiative balance of the Arctic environment in numerous ways (Carslaw et al., 2013; Ramanathan et al., 2001). Overall, different aerosol chemical species, as well as particle size and abundance, may determine the magnitude of the aerosol induced direct forcing. Furthermore, aerosols also constitute the seeds upon which cloud droplets form (Ramanathan et al., 2001). Improved understanding of the spatial and temporal variability of the microphysical properties of the aerosol in the Arctic is required in order to determine the magnitude and direction of future climate change in this important region.

The Arctic aerosol has been shown to be highly variable. Broadly, over the Arctic region the aerosol mass, surface area and number size distribution properties are a strong function of season, and this seasonality is repeated from year to year (Freud et al., 2017; Nguyen et al., 2016; Tunved et al., 2013). It is well established that the Arctic winter and spring atmosphere is more heavily impacted by transport of air pollution from lower latitudes compared to summer (Heidam et al., 2004; Law and Stohl, 2007). The continent-derived winter and spring aerosols, known as Arctic haze, reach their maximum number concentration during late spring, approximately in April. The transition from the Arctic haze conditions to the lower aerosol loadings over the summer period is driven by increasing wet scavenging due to increasing temperatures over a period of about two weeks (Browse et al., 2012; Croft et al., 2016; Engvall et al., 2008). It is becoming increasingly evident that biogenic ultrafine (including freshly nucleated) particles dominate ambient aerosols in Arctic areas during summer (Dall´Osto et al., 2017a; Dall´Osto et al., 2017c). Occasionally long-range pollution transport events also occur during summer (Iziomon et al., 2006; O'Neill et al., 2008). Towards the end of summer the intensity of sunlight decreases and, despite a low concentration of large particles, new particle formation comes to a halt as the production of nucleating vapors is too slow.

Aerosol number size distributions from multi-year measurements have been reported from different arctic research stations: Zeppelin (Tunved et al., 2013), Tiksi (Asmi et al., 2016), Alert (Croft et al., 2016), Barrow (Lathem et al., 2013) and Villum Research Station (VRS), Station Nord (Nguyen et al., 2016). All studies broadly converge in a similar scenario: the haze period characterized by a dominating accumulation mode aerosol (March–May), is followed by the sunlit summer with high concentration of small particles (June–August). The remaining year is characterized by low concentration of accumulation mode particles and negligible abundance of ultrafine (<100 nm) particles (September–February).

Despite this, information on different types of aerosol accumulation modes is scarce. Tunved et al. (2013) reported the occurrence of a typical accumulation mode geometric mean particle diameter (Dp) of 161-185 nm during winter months (November to March) and 130-163 nm during April to October, at Zeppelin, Svalbard. Nguyen et al. (2016) reported that the larger Dp accumulation mode persists further into the summer at VRS, Greenland, than at Zeppelin, with a typical mode geometric mean diameter Dp of 167-179 nm for months November to May and 107-119 nm for months June to September. A recent inter-comparison of particle number size distributions observed at several Arctic stations by Freud et al. (2017) suggests variations between the different stations throughout the year. The most prominent differences are observed between the stations at Barrow and Zeppelin. Barrow features a wider accumulation mode, with higher concentrations and smaller Dp than Zeppelin in months September to May.

To the best of our knowledge, no long-term studies on Arctic aerosol have identified several distinctively different accumulation mode aerosols. In this study we provide further evidence that multiple accumulation mode aerosol clusters exist in the Greenlandic high Arctic, and that these are present at different proportions throughout the year. These accumulation mode aerosol clusters are characterized both physically and chemically, and statistically significant differences are highlighted. In conclusion, the aim of the present paper is to improve the understanding of Arctic aerosol accumulation modes, and to describe them in tandem with meteorological parameters, gaseous concentrations, aerosol chemical species and cloud condensation nuclei properties.

2 Methodology

2.1 Location

All the data presented in this work was recorded at Villum Research Station, Station Nord, Greenland. Located at 81° 36' N, 16° 40' W the station is situated in the most north-eastern part of Greenland, on the coast of the Fram Strait. The sampling took place about 2 km south-west of the main facilities of the Station Nord military camp in two different sampling stations. Measurements were shifted in summer 2015 from the original hut called "Flygers hut" to the new air observatory, 300 m west of "Flygers hut". The sampling locations are upwind from the station the vast majority of the time. Detailed descriptions of the site and analysis of predominant wind directions are available in Nguyen et al. (2016) and Nguyen et al. (2013).

2.2 Scanning Mobility Particle Sizer (SMPS)

We analyzed continuous Scanning Mobility Particle Sizer (SMPS) data collected in the period 2010-2016 in the size range of 9-915 nm in diameter. The sampling setup has been described in detail by Nguyen et al. (2016), with the difference that since summer 2015 the SMPS has been situated in the newly constructed air observatory measurement hut, described above. The instrument is custom-built with a Vienna-type medium column, similar to SMPS instruments described in Wiedensohler et al. (2012). Our SMPS used either a condensation particle counter (CPC) model TSI 3010 or model TSI 7220. To ensure correct functioning, volumetric flow rates, temperatures and relative humidity (RH) of the aerosol- and sheath flow were monitored, as well as inlet ambient pressure. No additional drying was performed, as the transition from the low ambient temperatures outside of the huts (-45 to +15 °C, yearly average -15 °C) to the heated inside (>20 °C) generally provides sufficient decrease of RH. The SMPS sample flow RH only in exceptional cases exceeded 35%. An algorithm according to Pfeifer et al. (2014) was used to invert the SMPS measurements. The resulting particle number size distribution series were quality controlled to ensure correct functioning of the instrument and absence of

influence from local pollution from near-by vehicles or by the military camp. Data was excluded from further analysis when these conditions were not met.

2.3 Concentrations of Gaseous Pollutants

O_3 and NO_x were measured using gas analyzers (API photometric O_3 analyser (M400), API chemiluminescence NOx analyzer (M200AU)). NO_x data was available for most of 2011-2012, whereas O_3 data was available throughout most of the study period.

2.4 Particulate Matter Properties

In the period from May 2011 to August 2013, observations of the aerosol light absorption coefficient were conducted using the multiangle absorption photometer (MAAP, Model 5012 Thermo Scientific), described in detail in Petzold and Schönlinner (2004). More information can be found in Massling et al. (2015). Soot particle aerosol mass spectrometer (Aerodyne, SP-AMS) was deployed for four months over the period February-June 2015. Further details can be found in Nielsen et al. (2017) (manuscript in preparation).

2.5 Meteorological Data

Wind speed and wind direction from a sonic anemometer were available from April 2011 to April 2013 (Sonic anemometer (METEK, USA-1)). Data coverage is poorer during the winter months due to frost on the anemometer.

2.6 Cloud Condensation Nuclei

Aerosol CCN activity was measured by a Cloud Condensation Nuclei Counter (CCN-100, DMT) during two field studies in 2016. The first campaign was from April to May and the second from August to September 2016. The CCN counter measurement cycle included 10 settings of supersaturation (SS) in the range 0.1-1.0% SS and one at maximum reachable SS (~2% SS). The temperature gradient in the CCN column was allowed to stabilize for 5 min before recording measurements. However, 15 min. stabilizing time was used when resuming to 0.1% SS from the highest reachable SS. The measurement recording time was 5 min in all cases. The total CCN measurement cycle duration thus was 120 min. At the highest reachable SS all particles above 25 nm are assumed to activate as CCN. The CCN concentration at this SS was utilized to calibrate the total detectable particle concentration by the CCN counter, relative to that inferred from the SMPS. The instrument SS was calibrated at the beginning and end of each of the two field studies at 0.1-0.47% SS, resulting in four total SS calibrations during the whole CCN measurement period. Following the conclusion of the campaigns, additional SS calibrations were undertaken to verify that the calibrations made during the field studies were linear and valid ranging up to 1% SS. During these SS calibrations, CCN activation Dp (Dp_{crit}) of monodisperse ammonium sulfate aerosol was determined. The E-AIM model (Clegg et al., 1992; Wexler and Clegg, 2002) and the Köhler equation (Kohler, 1936) was used to calculate the corresponding real SS (SS_{calc}), which then was compared to the set SS on the CCN counter (SS_{set}). Combining the data from all performed SS calibrations yielded a linear relationship between SS_{calc} and SS_{set}. This was determined by linear least squares fitting. CCN data was quality controlled on the basis of achievement and stability of column temperature gradients, tolerances to temperature differences inside the instrument and stability of sample- and sheath air flows. By assuming chemical homogeneity of the measured aerosol population, critical activation diameters were calculated by sequential downwards integration of SMPS number size distributions until the following condition was satisfied (equation 1) (Kristensen et al., 2016; Jurányi et al., 2010):

$$\int_{Dp_{crit}}^{Dp_{max}} n_N(Dp)dDp = N_{CCN} \qquad \text{(equation 1)}$$

Where Dp_{max} is the maximum Dp measured by the SMPS, n_N is the particle number size distribution and N_{CCN} is the corresponding measured CCN number concentration. Internal particle losses of the CCN counter were accounted for when determining Dp_{crit}. This was done by applying a particle size dependent transmission curve for the CCN counter, published by Rose et al. (2010) to the SMPS number size distributions.

2.7 Aerosol Size Distribution Statistical Analysis

SMPS data from a total of 1,717 days distributed over the 7 years were examined by k-means analysis according to the methodology in Beddows et al. (2009). Eight clusters were selected based on the best compromise between Silhouette Width (0.43) and Dunn Index ($1.6 \cdot 10^{-3}$). The time series of these clusters were inspected to see if any could be merged and they proved to be separable. To each day of the data period the respective dominant cluster was assigned. Of the identified eight clusters, three are related to a dominant and distinct accumulation mode aerosol. The climate-relevant characteristics of these accumulation mode clusters are discussed in detail in this study. In total, the accumulation mode clusters are dominant on 56% of the days in the data period, while the remaining five clusters were dominant 44% of the time. The five remaining clusters are related to ultrafine particle modes (<100 nm) and are described elsewhere (Dall´Osto et al., 2017b). Size distribution parameters were obtained by fitting of log-normal functions to the average distributions. For each accumulation mode cluster, the average and median values of all measured parameters were calculated from the data obtained during the days the respective cluster was observed. To increase robustness towards outliers, the upper and lower 1-percentile from all utilized datasets were removed.

Results and Discussion

3.1 K-means Clustering Results

Fig. 1a shows the annual variation of the sum of the three accumulation categories with respect to their abundance relative to the sum of the five ultrafine ones (Dall´Osto et al., 2017b). The main difference between the ultrafine and the accumulation categories is in having the majority of $N_{9\text{-}915nm}$ in particle sizes lower and higher than 100nm, respectively. It can clearly be seen that the accumulation categories dominate the winter times (January-March, 89-91%), whereas they present a minimum in summer months (June-August, 1-5%). **Fig. 1b** shows the seasonality of each accumulation category, represented by the occurrence of each accumulation category during each month of the year. The three particle size distribution accumulation mode categories show very different seasonality for multiple reasons, including different meteorology and different biological ocean activity throughout the year as well as different anthropogenic influences over time. The three accumulation mode categories are termed *Haze*, *Bimodal* and *Aged*, based mainly on the temporal trends and aerosol size distributions. Additionally, it is important to note that chemical and physical parameters associated with each individual category are presented in the following sections - supporting the assigned terminology.

Fig. 1b shows that during July and August - where ultrafine categories dominate the particle number size distribution - the remaining accumulation aerosols mode categories consist solely of the *Bimodal* category. By contrast, during the months September and October its occurrence decreases while the *Aged* category reaches its maximum relative occurrence. The *Aged* category is largely absent from February to August. In the months November to April the *Haze* category is dominant, reaching its maximum occurrence in April.

The aerosol number and volume size distributions of the three accumulation aerosol categories are shown in **Fig. 2a** and **2b**, respectively. The *Haze* category appears with the highest total number concentration of the three categories. Its number size distribution peaks at Dp = 173 nm, and is unimodal in appearance. The *Bimodal* category depicts a larger mode that peaks at Dp = 150 nm, which accounts for 53% of its average total particle number concentration. The smaller mode around Dp = 38 nm accounts for the remaining 47% of average total particle number concentration. The *Aged* category is unimodal, with the maximum number concentration at Dp = 213 nm. The size range of our SMPS measurements was limited to the maximum size bin of 915 nm, leaving the particle volume size distributions incomplete (**Fig. 2b**). It appears that the *Haze* and *Aged* categories have roughly equal total volume concentrations in the measured range, whereas the *Bimodal* category had a significantly lower volume concentration in this range.

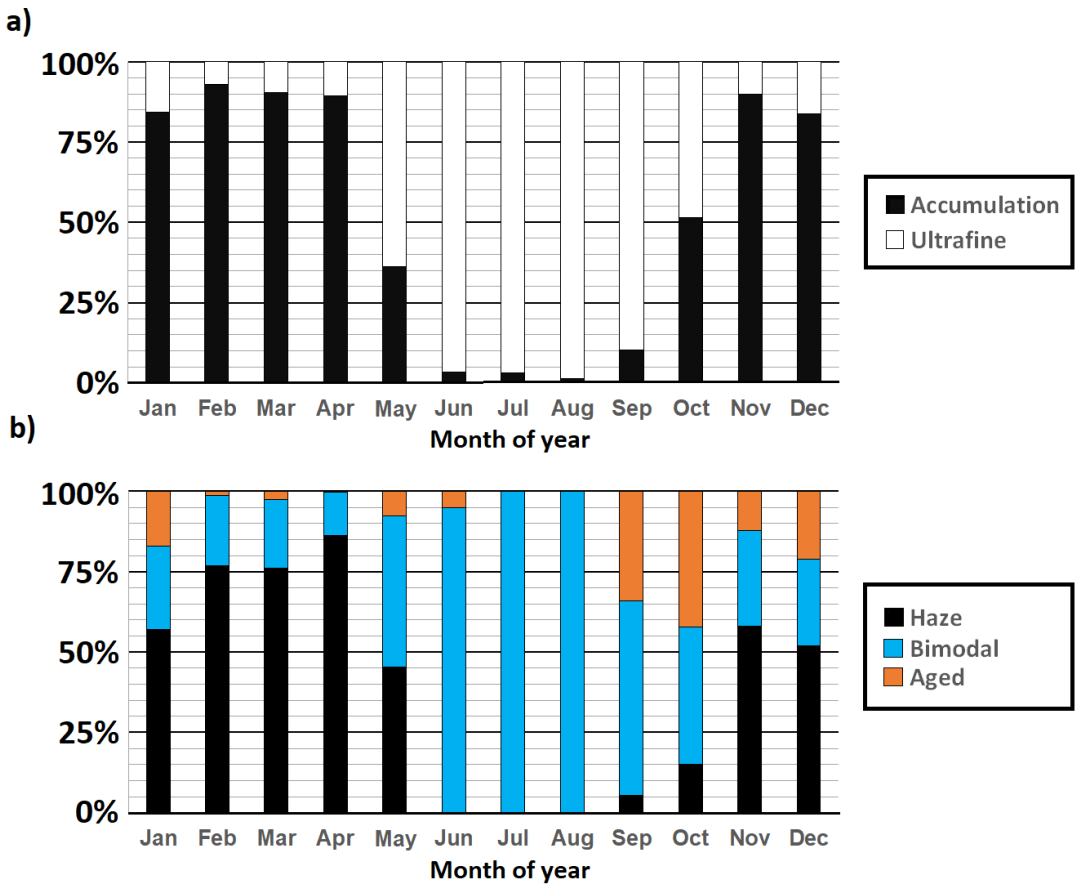

Fig. 1. (a) Ultrafine (<100nm) and Accumulation (>100nm) aerosol category occurrence presented as monthly averages (period 2010-2017). (b) Annual variation of the three accumulation mode aerosol categories only.

The aerosol size distributions presented in **Fig. 2** are obtained from the k-means clustering carried out with daily resolution. In general, aerosol number size distributions appear very stable over the days, allowing a classification of these distributions based on 24 hour averages. This can also be supported by the fact that same aerosol categories often appear in consecutive days. A strong variation in daily aerosol number size distribution is only observed during nucleation events, because this is the nature of the underlying process. The calculated average condensation sink (CS) (Dall'Osto et al., 2013) presented by the three accumulation categories was 1.12 * 10^{-3}, 0.71 * 10^{-3} and 0.89 * 10^{-3} s^{-1} for the *Haze*, *Bimodal* and *Aged*, respectively. These daily average CS values are well above those calculated for days characterized by ultrafine categories (1-8 * 10^{-4} s^{-1}) (Dall´Osto et al., 2017b).

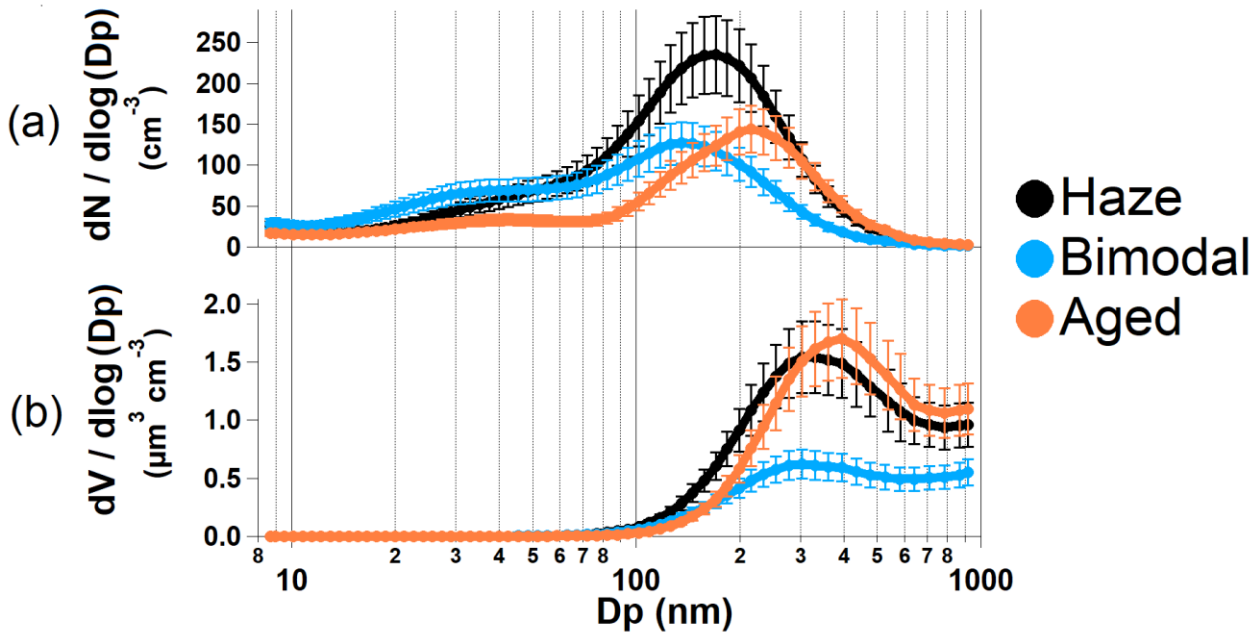

Fig. 2. Aerosol (a) number and (b) volume size distributions for the three accumulation categories.

3.2 Gas Concentrations and Meteorological Parameters

Daily median gaseous concentrations were calculated and compared with the appearance of accumulation aerosol categories (**Table 1**). NO_x was always found near the detection limit of 0.2 ppb. O_3 concentration medians were 32.9, 34.6 and 28.7 ppb for the categories

Haze, *Bimodal* and *Aged*, respectively. Median O_3 and NO_x concentrations did not show any diurnal profile, indicating that there is no varying influx of polluted air from the station premises to the measurement site. The above mentioned factors suggest that the examined accumulation categories are probably attributable to regional and long range transport, and not to local pollution.

Table 1 also shows the average meteorological parameters observed for each category. The *Haze* aerosol category was observed during episodes of high atmospheric pressure, low temperatures, relatively dry conditions and a high amount of incoming shortwave radiation. The *Bimodal* category was observed during episodes with higher temperature and lower atmospheric pressure, while the *Aged* category was observed at the highest temperatures, highest relative humidity, highest wind speed and lowest pressure. We find statistically significant differences (Wilcoxon signed-rank, $z < 0.05$) between all average parameters except for the irradiance and pressure of the *Bimodal* and *Aged* categories, and between the average wind speed of the *Haze* and *Aged* categories. These findings agree well with the expectation that Arctic haze is most prominent during late winter and early spring, when conditions are usually sunny and cold. The *Aged* category on the other hand is usually observed during cloudy and humid weather conditions during autumn or during winter, when sunlight is absent. We calculated about 10,300 air mass back trajectories aiming to shed light on possible source regions. A “modal” air mass back trajectory for each number size distribution cluster was calculated by averaging all the back trajectories calculated with arrival dates corresponding to days with assignment of a k-Mean cluster. Using HYSPLIT4 (with revision made in February 2016), five day backward trajectories were calculated from 2010 to 2016 using arrival hours of 00:00, 06:00, 12:00 and 18:00 and an arrival height of 10 m. Unfortunately, no robust differences were found among the accumulation categories.

Accumulation aerosol category	**O_3 (ppb)**	**T (° C)**	**RH (%)**	**Radiation (W/m^2)**	**Pressure (hPa)**	**Wind speed (m/s)**
Haze	32.9 (±6.4)	-18.9 (±6.2)	74.1 (±6.6)	60.4 (±110.6)	1017.4 (±8.7)	3.1 (±2.2)
Bimodal	34.6 (±8.2)	-16.0 (±10.0)	74.4 (±8.1)	48.0 (±110.9)	1013.7 (±10.2)	3.0 (±2.3)
Aged	28.7 (±7.6)	-12.2 (±9.7)	80.0 (±4.1)	18.2 (±72.3)	1012.2 (±10.0)	3.3 (±2.7)

Table 1

Median Ozone concentration and average meteorological parameters (Temperature, Relative Humidity, Radiation, Pressure and Wind speed) for the three accumulation aerosol categories.

3.3 Chemical Composition

Long-term (two year period between 2011 and 2013) MAAP (Multi Angle Absorption Photometer) measurements of black carbon (BC) mass concentration were compared with our accumulation aerosol classification (Fig 3a). The highest average BC concentration of 77 ng m^{-3} was found concurrent with the *Haze* category. By contrast, the lowest (27 ng m^{-3}) was found with the *Bimodal* category. Intermediate values were found for the *Aged* cluster (55 ng m^{-3}). This trend is in agreement with five months of SP-AMS measurements conducted in 2016 (Fig 3a). Arctic marine air masses are expected to be associated with pristine clean conditions, with BC concentrations smaller than 15 ng m^{-3}. We conclude from the BC data that all three accumulation categories occurred under perturbed natural conditions, which to some extent are influenced by anthropogenic emissions. Previously measured atmospheric black carbon concentrations in Northeast Greenland averaged 67±71 ng m^{-3} in winter and 11±9 ng m^{-3} in summer (Massling et al., 2015). Our study shows that aerosol number size distributions characterized by dominant accumulation modes are associated with average BC concentrations in the range of 27-77 ng m^{-3}.

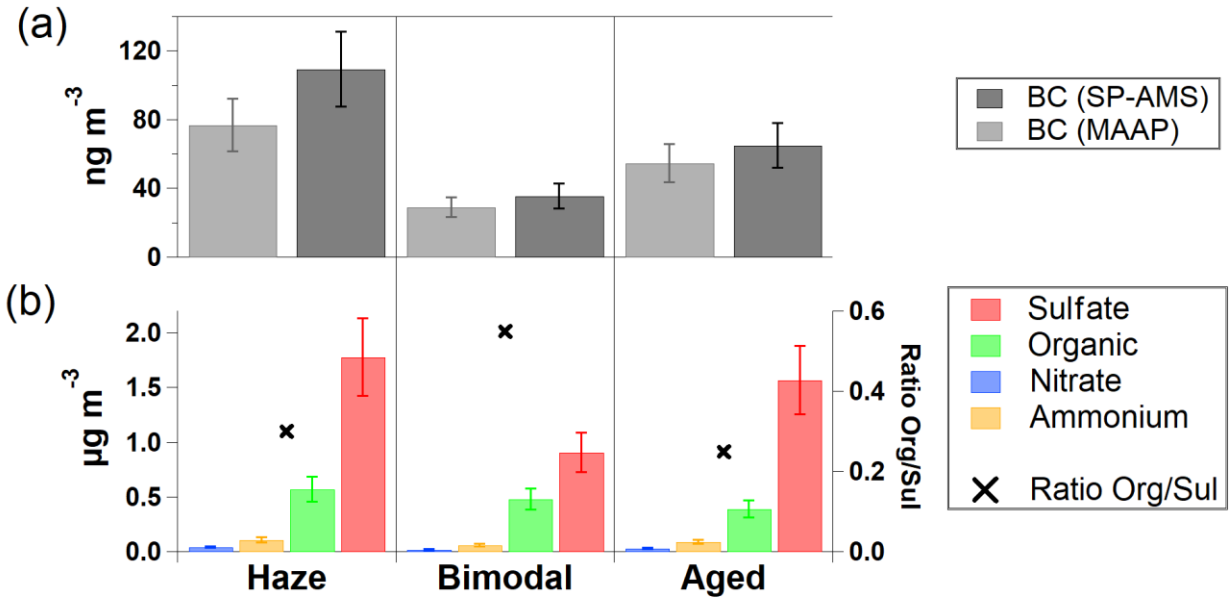

Fig. 3. (a) Aerosol black carbon mass derived from the MAAP and SP-AMS. (b) AMS-derived sulfate, organic, nitrate and ammonium mass as a function of the three aerosol accumulation categories.

Additional information can be obtained by comparing our accumulation aerosol categories with aerosol chemical measurements obtained by SP-AMS. **Fig. 3b** shows average mass concentrations obtained for nitrate, sulfate, organics and ammonium. The *Haze* category presented high concentrations of sulfate (1.79 µg m^{-3}) and organics, (0.57 µg m^{-3}). This category is also associated with the highest average concentrations of nitrate (0.04 µg m^{-3}) and ammonium (0.11 µg m^{-3}). By contrast, the *Bimodal* category concurs with lower concentrations of sulfate (0.91 µg m^{-3}), organics (0.48 µg m^{-3}), nitrate (0.02 µg m^{-3}) and ammonium (0.06 µg m^{-3}). The *Aged* category features 1.57 µg m^{-3} and 0.39 µg m^{-3} of sulfate and organics, respectively, and 0.03 µg m^{-3} and 0.09 µg m^{-3} of nitrate and ammonium, respectively. The very low nitrate concentrations for the *Bimodal* and *Aged* categories are below the limit of quantification. A statistically significant difference (Wilcoxon signed-rank, $z < 0.05$) exists between the basic chemical composition of the three categories, except for nitrate, ammonium and organics between the *Haze* and the *Aged* aerosols.

Previous studies at Villum Research Station observed a positive correlation ($R^2 = 0.72$) between BC and sulfate concentrations over the years 2011 to 2013 (Massling et al., 2015), suggesting that the transport of combustion-derived BC-rich particles to the Arctic

was accompanied by aging of the aerosols through condensational processes. It has also previously been shown that the sulfate concentrations observed at the VRS station are dominantly affected by anthropogenic emissions and to a lesser extent by sea spray (Heidam et al., 2004; Nguyen et al., 2013). However, our new analysis with a much higher resolution (hourly aerosol number size distributions, versus previously 7 days off-line filter measurements) allows to separate the three accumulation mode categories. For all the analyzed chemical components, the largest aerosol loadings are found in the *Haze* category, and the lowest in the *Bimodal* category. Additional important information can be drawn from the ratios among different chemical components. For example, the ratios of organics to BC in the *Haze* and *Aged* categories were very similar (7.1 and 7.4). By profound contrast, the ratio was 18 for the *Bimodal* aerosol category. A similar pattern was found for the ratio of organics to sulfate average mass concentrations (**Fig. 3b**): the ratio of the *Bimodal* category (0.55) is higher than the ratios of the other two categories (*Haze* and *Aged*) (0.25-0.3). Therefore, the *Bimodal* aerosols are enriched with organic matter and anti-correlation with BC content. Due to the usually low concentrations of aerosols over the inner Arctic pack ice area in summer, biogenic natural particle sources have been emphasized to be more important than transport from continental sources. Biogenic primary ultrafine aerosols include micro-colloids shown to behave as polymeric gels (Chin et al., 1998; Leck and Bigg, 2005; Orellana et al., 2011). These are produced by phytoplankton and sea ice algae as biological secretions. A number of studies have also reported in situ formation of secondary new aerosols in the Arctic, which mostly involve new particle formation from natural emissions of volatile species and their subsequent oxidation to low volatility compounds (Dall´Osto et al., 2017a; Nguyen et al., 2016; Tunved et al., 2013). It is likely that the organic enrichment detected in the *Bimodal* cluster results from the combination of primary and secondary aerosols of biological origin.

3.3 CCN Properties

The net climate impact of atmospheric aerosols depends on their number size distribution and chemical composition (Rosenfeld, 2006). In particular, particle size (Anttila et al., 2012; Dusek et al., 2006) have been found to be the greatest controlling factor in cloud

condensation nuclei (CCN) efficiency. As the Arctic often is a CCN-limited regime, the variability of even low concentrations of CCN is important (Mauritsen et al., 2011).

We calculated average daily CCN concentrations corresponding to each accumulation aerosol cluster. **Fig. 4a** shows the CCN concentrations at different supersaturations (%) for two of the three clusters. *Aged* aerosols did not have enough associated CCN data and are not discussed hereafter. The *Haze* cluster presented total CCN concentrations of around 80±20 cm^{-3} at all supersaturations. By contrast, a clear gradient was seen for the *Bimodal* cluster, with CCN concentrations increasing from 43 cm^{-3} to 88 cm^{-3} as SS increased from 0.1 to 1.0%. No statistically significant difference was found between CCN concentrations for the two different accumulation clusters at SS above 0.3%. This is very interesting, given the higher $N_{9\text{-}915nm}$ in *Haze* than in *Bimodal* aerosols (**Fig. 2a**). Most CCN-active particles are typically sized between 50 and 150 nm diameter; traditionally a typical cloud condensation nucleus (CCN) is considered to have a minimum diameter of about 100 nm. Considering this threshold size, we find an average $N_{>100nm}$ concentration of 109 cm^{-3} and 54 cm^{-3} in the *Haze* and *Bimodal* clusters, respectively; whereas concentrations of $N_{<100nm}$ are similar (54 cm^{-3} and 59 cm^{-3}, respectively; **Fig. 2a**). **Fig. 4b** shows the CCN activated fraction (i.e. the ratio of CCN activated at a given supersaturation over the total particle concentration at sizes Dp > 25 nm) for the two aerosol clusters. For the *Haze* aerosols, the CCN activated fraction (CCN/CN_{25nm}) increases from 0.68 to 0.81 when SS increases from 0.1 to 0.4%; thereafter it increases only slowly to 0.85 at a maximum SS of 1.0%. By contrast, the CCN activated fraction of the *Bimodal* aerosols increases from 0.42 to 0.71 with SS increasing from 0.1 to 0.4%, and from 0.71 to 0.88 when SS increases from 0.5% to 1.0%. As the smaller mode accounts for 47% of the *Bimodal* particle number, this implies that these smaller particles must contribute to the CCN concentrations even at relatively low supersaturations. Indeed, **Fig. 4c** shows the critical activation diameter as calculated by equation 1. The Dp_{crit} of *Haze* accumulation mode aerosols slightly decreases across increasing SS, from 129 nm at SS 0.1% to 91 nm at SS 0.35% to 82 nm at SS 1.0%. By contrast, the Dp_{crit} of *Bimodal* aerosols decreases more sharply from 128nm at SS 0.1% to 71 nm at SS 0.35% to as small as 42 nm at SS 1%.

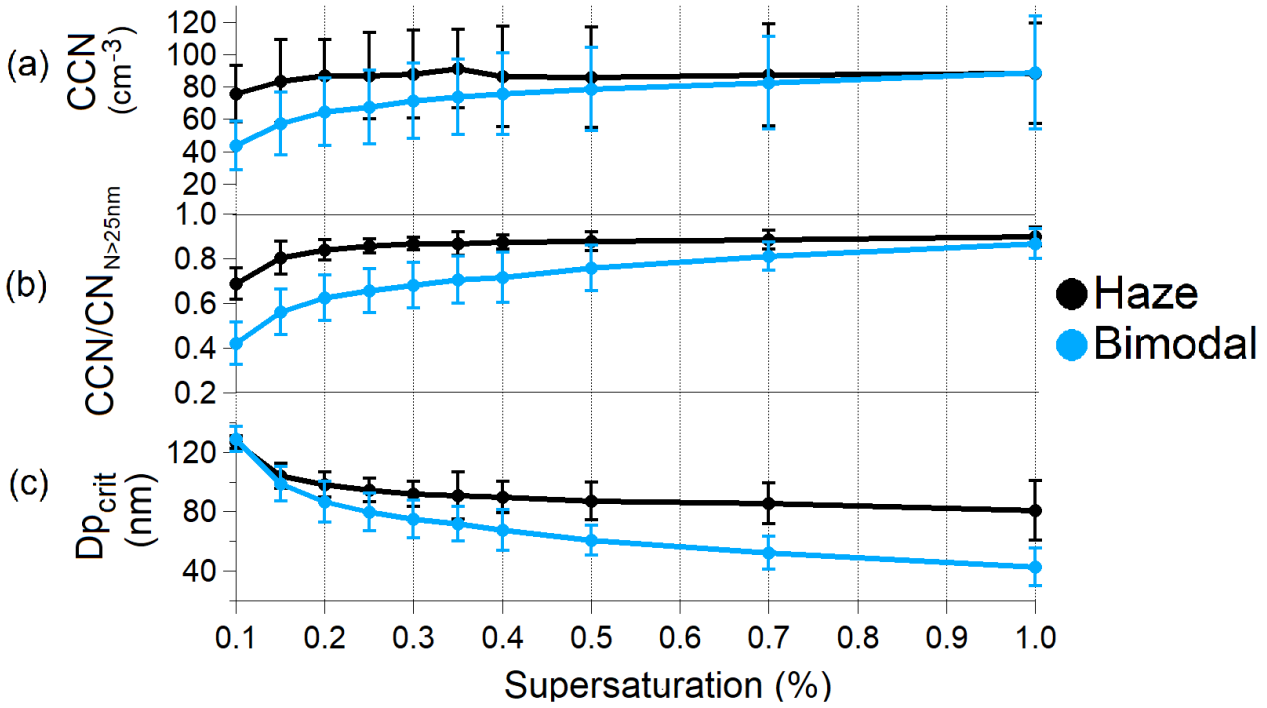

Fig. 4. CCN properties for the *Haze* and *Bimodal* category as function of supersaturation. (a) Total CCN concentration. (b) Fraction of CCN activated particles larger than 25 nm. (c) Critical CCN activation diameter Dp_{crit}.

Given the different average BC concentrations (22 and 75ng m^{-3}, respectively), *Haze* can be associated mainly with Arctic Haze anthropogenic events, while *Bimodal* being representative of summer months and mostly of natural imprinting.

Aerosol particles smaller than 100 nm in diameter are often considered too small to activate to cloud droplets. This result comes from the assumption that the cooling mechanisms are not efficient enough to generate supersaturations required to activate the smaller particles in liquid clouds, thus the kelvin effect acts as the limiting factor from a microphysical perspective (Browse et al., 2014; Garrett et al., 2004; Leaitch et al., 2013; Zhao and Garrett, 2015). However, in the clean environment often found in the Arctic during summer, the absence of larger particles may lower water uptake rates during droplet formation, which increases SS, thus enabling smaller particles to become cloud droplets. In addition, we found relatively low activation diameters for arctic aerosols with strong abundance in summer months. Our study strongly supports recent findings by Leaitch et al. (2016) that 20-100 nm particles from natural sources can have a broad impact on CCN numbers in Arctic environments.

3.3 Summary, Implications and Conclusions

Mass concentrations of atmospheric aerosols in the Arctic are higher during winter compared to summer due to differences in transport of anthropogenic particles and wet scavenging (Stohl, 2006). By contrast, total aerosol number concentrations in the Arctic are often found similar throughout the period of March-September (Tunved et al., 2013). However, the high concentrations in spring (March–April) are almost exclusively governed by accumulation mode aerosols, while the high summer concentrations are associated with elevated numbers of Aitken mode particles and frequent new particle formation events. So far, differences within the accumulation mode aerosol types over seasons have not been studied, and this was the main objective of our study. Based on k-means cluster analysis of seven years of aerosol number size distributions, we identified eight distribution aerosol size categories. Five were associated with aerosol modes dominated by the ultrafine (<100nm) sizes and are described elsewhere (Dall´Osto et al., 2017b). The remaining three aerosol categories were dominated by the accumulation mode particles (>100 nm) and were named *Haze* (dominant 32% of the time), *Aged* (14%) and *Bimodal* (6%). We found the accumulation mode categories to comprise the ambient aerosol number size distributions at the high Arctic site of Villum research Station more than half of the time.

Accumulation mode categories presented very distinct chemical and physical properties across seasons. *Haze* accumulation aerosols show a single mode size distribution (150 nm), peaking in February-April; *Aged* aerosols show a single mode at 213 nm, peaking in September-October; and *Bimodal* aerosols show two modes at 38 nm and 150 nm, peaking in June-August. A first conclusion that can be drawn from the current study is that a typical accumulation mode does not exist, and profound differences are found especially between the Arctic Haze period and the summer period. Surprisingly the largest Dp accumulation mode is not straightly associated with the Arctic Haze, but it is found during fall and associated with humid conditions. A clear unimodal distribution is never found in accumulation aerosols during the months of July and August (and most of June); rather, it

is mostly *Bimodal*, implying that aerosols originating from long-range transport to the Arctic coexist with a smaller mode formed locally to regionally.

Considerable attention has been given to the role of anthropogenic and biomass burning (BB) particles as warming agents in the Arctic (UNEP, 2011). Black carbon contributes to Arctic warming, yet sources of Arctic BC and their geographic origins remain uncertain (Xu et al., 2017). BC particles and especially aged BC particles affect the radiation budget directly by scattering and absorbing incoming solar radiation (Massling et al., 2015). Sensitivity simulations (Xu et al., 2017) suggest that anthropogenic emissions in eastern and southern Asia have the largest effect on the Arctic BC column burden both in spring (56%) and annually (37%). By investigating the relationship between aerosol categories and black carbon concentration, we have previously demonstrated that pristine clean conditions (BC < 18 ng m^{-3}) co-occur with ultrafine-sized dominating aerosols (Dall´Osto et al., 2017b). The present analysis of accumulation aerosol categories shows that number size distributions characterized by dominant accumulation modes are associated with average BC concentrations in the range of 27-77 ng m^{-3}, i.e., associated to a varying extent with contributions of anthropogenic pollutants mainly originated from northern Eurasia. Only when lower-end BC concentrations occur over the summer (in the order of 27 ng m^{-3}) the *Bimodal* category, characterized by smaller aerosols of biogenic origin, becomes dominant.

When including chemical components in the analysis, further conclusions can be drawn. Sulfate is the dominant component in the Arctic haze (Massling et al., 2015; Udisti et al., 2016); indeed we found the highest concentrations associated with the *Haze* category. However, sulfate is also produced by the oxidation of dimethyl sulfide (DMS) (Simo, 2001). DMS is of marine origin, and is produced in the upper ocean via interactions of multiple biological processes (Gali and Simo, 2015). During the Arctic summer, the impact of the anthropogenic source is lower (42%), with a contribution comparable to that coming from biogenic emissions (35%), which reaches absolute and percentage values about two times higher than those measured in spring (Udisti et al., 2016). Nevertheless, sulfate concentrations observed at Villum Research Station in summer time are relatively small compared to winter and spring when anthropogenic sources are the main contributor

(Heidam et al., 1999). The highest ratio of organics/sulfate and organics/BC among the accumulation mode aerosol categories was found in the *Bimodal* one. It is probable that such organic enhancement is associated with the smaller mode (38 nm). The origin of this mode is likely to be a combination of secondary aerosol formation of marine biological origin from the open waters between ice floes (Dall´Osto et al., 2017a, b), but also from fragmentation and/or dispersion of primary marine polymer gels also originated in water adjacent to the ice (Leck and Bigg, 2005; Orellana et al., 2011).

Cloud condensation nuclei are a functionally important fraction of the atmospheric aerosol, because they influence cloud microphysical and radiative properties, and consequently the aerosol indirect radiative forcing (IPCC, 2014). Low level clouds are one of the major players controlling the radiative balance in the Arctic. At the most fundamental level, understanding the processes that determine cloud properties from microscale to global scale requires information of which particles actually form cloud droplets under various conditions. The effect of the background aerosol on liquid clouds has been identified as one of the most important factors for reducing uncertainty in the aerosol cloud albedo effect (Carslaw et al., 2013). Moreover, the effectiveness of particles smaller than 100 nm for cloud droplet nucleation is a large factor in that uncertainty. During summer the Arctic is thought to be relatively free of anthropogenic influence, which means that dominantly only particles from natural sources determine cloud droplet formation. This study shows that, despite anthropogenic influence is maintained moderate through most of the summer, natural sources have indeed a significant impact on particle number, and on facilitating aerosol activation to cloud droplets and thus cloud formation. Further integrated studies with joint multi-component observations are warranted.

Acknowledgements

The study was supported by the Spanish Ministry of Economy through project BIO-NUC (CGL2013-49020-R), and by the EU though the FP7-PEOPLE-2013-IOF programme (Project number 624680, MANU – Marine Aerosol NUcleations). The National Centre for Atmospheric Science NCAS Birmingham group is funded by the UK Natural Environment

Research Council. Thanks to the British Atmospheric Data Centre, which is part of the NERC National Centre for Atmospheric Science (NCAS), for the calculation of trajectories and access to ECMWF data. This work was financially supported by the Danish Environmental Protection Agency with means from the MIKA/DANCEA funds for Environmental Support to the Arctic Region, which is part of the Danish contribution to "Arctic Monitoring and Assessment Program" (AMAP) and the Danish research project "Short lived Climate Forcers" (SLCF), and the Danish Council for Independent Research (project NUMEN, DFF-FTP-4005-00485B). The findings and conclusions presented here do not necessarily reflect the views of the Agency. This work was also supported by the Nordic Centre of Excellence (NCoE) Cryosphere-Atmosphere Interactions in a Changing Arctic Climate (CRAICC). The Villum Foundation is acknowledged for funding the construction of Villum Research Station, Station Nord. The authors are also grateful to Bjarne Jensen, Keld Mortensen and the staff at Station Nord for their excellent and unwavering support.

References

AMAP (2011), AMAP: Snow, Water, Ice and Permafrost in the Arctic (SWIPA), Climate Change and the Cryosphere, 538 pp, OSLO.

Anttila, T., D. Brus, A. Jaatinen, A. P. Hyvarinen, N. Kivekas, S. Romakkaniemi, M. Komppula, and H. Lihavainen (2012), Relationships between particles, cloud condensation nuclei and cloud droplet activation during the third Pallas Cloud Experiment, *Atmospheric Chemistry and Physics*, *12*(23), 11435-11450, doi:10.5194/acp-12-11435-2012.

Asmi, E., et al. (2016), Aerosol size distribution seasonal characteristics measured in Tiksi, Russian Arctic, *Atmospheric Chemistry and Physics*, *16*(3), 1271-1287, doi:10.5194/acp-16-1271-2016.

Beddows, D. C. S., M. Dall'Osto, and R. M. Harrison (2009), Cluster Analysis of Rural, Urban, and Curbside Atmospheric Particle Size Data, *Environmental Science & Technology*, *43*(13), 4694-4700, doi:10.1021/es803121t.

Browse, J., K. S. Carslaw, S. R. Arnold, K. Pringle, and O. Boucher (2012), The scavenging processes controlling the seasonal cycle in Arctic sulphate and black carbon aerosol, *Atmospheric Chemistry and Physics*, *12*(15), 6775-6798, doi:10.5194/acp-12-6775-2012.

644 Browse, J., K. S. Carslaw, G. W. Mann, C. E. Birch, S. R. Arnold, and C. Leck (2014), The
645 complex response of Arctic aerosol to sea-ice retreat, *Atmospheric Chemistry and*
646 *Physics*, *14*(14), 7543-7557, doi:10.5194/acp-14-7543-2014.
647 Carslaw, K. S., et al. (2013), Large contribution of natural aerosols to uncertainty in indirect
648 forcing, *Nature*, *503*(7474), 67-71, doi:10.1038/nature12674.
649 Chin, W. C., M. V. Orellana, and P. Verdugo (1998), Spontaneous assembly of marine dissolved
650 organic matter into polymer gels, *Nature*, *391*(6667), 568-572.
651 Clegg, S. L., K. S. Pitzer, and P. Brimblecombe (1992), Thermodynamics of Multicomponent,
652 Miscible, Ionic-Solutions .2. Mixtures Including Unsymmetrical Electrolytes, *Journal*
653 *of Physical Chemistry*, *96*(23), 9470-9479, doi:10.1021/j100202a074.
654 Croft, B., R. V. Martin, W. R. Leaitch, P. Tunved, T. J. Breider, S. D. D'Andrea, and J. R. Pierce
655 (2016), Processes controlling the annual cycle of Arctic aerosol number and size
656 distributions, *Atmospheric Chemistry and Physics*, *16*(6), 3665-3682.
657 Dall'Osto, M., X. Querol, A. Alastuey, C. O'Dowd, R. M. Harrison, J. Wenger, and F. J. Gomez-
658 Moreno (2013), On the spatial distribution and evolution of ultrafine particles in
659 Barcelona, *Atmospheric Chemistry and Physics*, *13*(2), 741-759, doi:10.5194/acp-13-
660 741-2013.
661 Dall´Osto, M., et al. (2017a), Arctic sea ice melt leads to atmospheric new particle formation,
662 *Scientific Reports*, *7*(1), 3318, doi:10.1038/s41598-017-03328-1.
663 Dall´Osto, M., R. Lange, C. Geels, D. C. S. Beddows, R. M. Harrison, R. Simo, D. Boertmann, H.
664 Skov, and A. Massling (2017b), Open pack ice drives new particle formation in North
665 East Greenland, *Scientific Reports, Under review*.
666 Dall´Osto, M., et al. (2017c), Antarctic sea ice region as a source of biogenic organic nitrogen in
667 aerosols, *Scientific Reports*, *7*, doi:10.1038/s41598-017-06188-x.
668 Dusek, U., et al. (2006), Size matters more than chemistry for cloud-nucleating ability of aerosol
669 particles, *Science*, *312*(5778), 1375-1378, doi:10.1126/science.1125261.
670 Engvall, A. C., R. Krejci, J. Strom, R. Treffeisen, R. Scheele, O. Hermansen, and J. Paatero (2008),
671 Changes in aerosol properties during spring-summer period in the Arctic troposphere,
672 *Atmospheric Chemistry and Physics*, *8*(3), 445-462.
673 Freud, E., R. Krejci, P. Tunved, R. Leaitch, Q. T. Nguyen, A. Massling, H. Skov, and L. Barrie
674 (2017), Pan-Arctic aerosol number size distributions: seasonality and transport
675 patterns, *Atmospheric Chemistry and Physics*, *17*(13), 8101-8128, doi:10.5194/acp-
676 17-8101-2017.
677 Gali, M., and R. Simo (2015), A meta-analysis of oceanic DMS and DMSP cycling processes:
678 Disentangling the summer paradox, *Global Biogeochemical Cycles*, *29*(4), 496-515,
679 doi:10.1002/2014gb004940.
680 Garrett, T. J., C. Zhao, X. Dong, G. G. Mace, and P. V. Hobbs (2004), Effects of varying aerosol
681 regimes on low-level Arctic stratus, *Geophysical Research Letters*, *31*(17),
682 doi:10.1029/2004gl019928.
683 Heidam, N. Z., J. Christensen, P. Wahlin, and H. Skov (2004), Arctic atmospheric contaminants in
684 NE Greenland: levels, variations, origins, transport, transformations and trends 1990-
685 2001, *Science of the Total Environment*, *331*(1-3), 5-28,
686 doi:10.1016/j.scitotenv.2004.03.033.
687 Heidam, N. Z., P. Wahlin, and J. H. Christensen (1999), Tropospheric gases and aerosols in
688 northeast Greenland, *Journal of the Atmospheric Sciences*, *56*(2), 261-278,
689 doi:10.1175/1520-0469(1999)056<0261:Tgaain>2.0.Co;2.
690 IPCC (2014), Climate Change 2014: Impacts, Adaptation, and vulnerability.

691 Iziomon, M. G., U. Lohmann, and P. K. Quinn (2006), Summertime pollution events in the Arctic
692 and potential implications, *Journal of Geophysical Research-Atmospheres*, *111*(D12),
693 doi:10.1029/2005jd006223.
694 Jurányi, Z., M. Gysel, E. Weingartner, P. F. DeCarlo, L. Kammermann and U. Baltensperger
695 (2010), Measured and modelled cloud condensation nuclei number concentration at
696 the high alpine site Jungfraujoch, *Atmospheric Chemistry and Physics*, *10*(16), 7891-
697 7906, doi: 10.5194/acp-10-7891-2010
698 Kohler, H. (1936), The nucleus in and the growth of hygroscopic droplets., *Transactions of the*
699 *Faraday Society*, *32*(2), 1152-1161, doi:10.1039/tf9363201152.
700 Kristensen, T. B., T. Müller, K. Kandler, N. Benker, M. Hartmann, J. M. Prospero, A.
701 Wiedensohler and F. Stratmann (2015), Properties of cloud condensation nuclei
702 (CCN) in the trade wind marine boundary layer of the western North Atlantic,
703 *Atmospheric Chemistry and Physics*, *16*(4), 2675-2688, doi: 10.5194/acp-16-2675-
704 2016
705 Lathem, T. L., A. J. Beyersdorf, K. L. Thornhill, E. L. Winstead, M. J. Cubison, A. Hecobian, J. L.
706 Jimenez, R. J. Weber, B. E. Anderson, and A. Nenes (2013), Analysis of CCN activity
707 of Arctic aerosol and Canadian biomass burning during summer 2008, *Atmospheric*
708 *Chemistry and Physics*, *13*(5), 2735-2756, doi:10.5194/acp-13-2735-2013.
709 Law, K. S., and A. Stohl (2007), Arctic air pollution: Origins and impacts, *Science*, *315*(5818),
710 1537-1540, doi:10.1126/science.1137695.
711 Leaitch, W. R., L. Huang, A. M. Macdonald, S. Sharma, D. Toom-Sauntry, K. von Salzen, and J. R.
712 Pierce (2013), A Comparison of Measurements and Global Model Simulations of the
713 Atmospheric Aerosol at Two Remote Sites, *Nucleation and Atmospheric Aerosols*,
714 *1527*, 511-514, doi:10.1063/1.4803318.
715 Leaitch, W. R., et al. (2016), Effects of 20-100nm particles on liquid clouds in the clean
716 summertime Arctic, *Atmospheric Chemistry and Physics*, *16*(17), 11107-11124,
717 doi:10.5194/acp-16-11107-2016.
718 Leck, C., and E. K. Bigg (2005), Biogenic particles on the surface microlayer and overlaying
719 atmosphere in the central Arctic Ocean during summer, *Tellus Series B-Chemical and*
720 *Physical Meteorology*, *57B*, 305-316.
721 Massling, A., I. E. Nielsen, D. Kristensen, J. H. Christensen, L. L. Sorensen, B. Jensen, Q. T.
722 Nguyen, J. K. Nojgaard, M. Glasius, and H. Skov (2015), Atmospheric black carbon
723 and sulfate concentrations in Northeast Greenland, *Atmospheric Chemistry and*
724 *Physics*, *15*(16), 9681-9692, doi:10.5194/acp-15-9681-2015.
725 Mauritsen, T., et al. (2011), An Arctic CCN-limited cloud-aerosol regime, *Atmospheric Chemistry*
726 *and Physics*, *11*(1), 165-173, doi:10.5194/acp-11-165-2011.
727 Nguyen, Q. T., M. Glasius, L. L. Sorensen, B. Jensen, H. Skov, W. Birmili, A. Wiedensohler, A.
728 Kristensson, J. K. Nojgaard, and A. Massling (2016), Seasonal variation of
729 atmospheric particle number concentrations, new particle formation and atmospheric
730 oxidation capacity at the high Arctic site Villum Research Station, Station Nord,
731 *Atmospheric Chemistry and Physics*, *16*(17), 11319-11336, doi:10.5194/acp-16-
732 11319-2016.
733 Nguyen, Q. T., H. Skov, L. L. Sorensen, B. J. Jensen, A. G. Grube, A. Massling, M. Glasius, and J.
734 K. Nojgaard (2013), Source apportionment of particles at Station Nord, North East
735 Greenland during 2008-2010 using COPREM and PMF analysis, *Atmospheric*
736 *Chemistry and Physics*, *13*(1), 35-49, doi:10.5194/acp-13-35-2013.
737 O'Neill, N. T., O. Pancrati, K. Baibakov, E. Eloranta, R. L. Batchelor, J. Freemantle, L. J. B.
738 McArthur, K. Strong, and R. Lindenmaier (2008), Occurrence of weak, sub-micron,

tropospheric aerosol events at high Arctic latitudes, *Geophysical Research Letters*, *35*(14), doi:10.1029/2008gl033733.

Orellana, M. V., P. A. Matrai, C. Leck, C. D. Rauschenberg, A. M. Lee, and E. Coz (2011), Marine microgels as a source of cloud condensation nuclei in the high Arctic, *Proceedings of the National Academy of Sciences of the United States of America*, *108*(33), 13612-13617, doi:10.1073/pnas.1102457108.

Petzold, A., and M. Schonlinner (2004), Multi-angle absorption photometry - a new method for the measurement of aerosol light absorption and atmospheric black carbon, *Journal of Aerosol Science*, *35*(4), 421-441, doi:10.1016/j.jaerosci.2003.09.005.

Pfeifer, S., W. Birmili, A. Schladitz, T. Muller, A. Nowak, and A. Wiedensohler (2014), A fast and easy-to-implement inversion algorithm for mobility particle size spectrometers considering particle number size distribution information outside of the detection range, *Atmospheric Measurement Techniques*, *7*(1), 95-105, doi:10.5194/amt-7-95-2014.

Ramanathan, V., P. J. Crutzen, J. T. Kiehl, and D. Rosenfeld (2001), Atmosphere - Aerosols, climate, and the hydrological cycle, *Science*, *294*(5549), 2119-2124, doi:10.1126/science.1064034.

Rose, D., A. Nowak, P. Achtert, A. Wiedensohler, M. Hu, M. Shao, Y. Zhang, M. O. Andreae, and U. Poschl (2010), Cloud condensation nuclei in polluted air and biomass burning smoke near the mega-city Guangzhou, China - Part 1: Size-resolved measurements and implications for the modeling of aerosol particle hygroscopicity and CCN activity, *Atmospheric Chemistry and Physics*, *10*(7), 3365-3383.

Rosenfeld, D. (2006), Atmosphere - Aerosols, clouds, and climate, *Science*, *312*(5778), 1323-1324, doi:10.1126/science.1128972.

Simo, R. (2001), Production of atmospheric sulfur by oceanic plankton: biogeochemical, ecological and evolutionary links, *Trends in Ecology & Evolution*, *16*(6), 287-294, doi:10.1016/S0169-5347(01)02152-8.

Stohl, A. (2006), Characteristics of atmospheric transport into the Arctic troposphere, *Journal of Geophysical Research-Atmospheres*, *111*(D11), doi:10.1029/2005jd006888.

Tunved, P., J. Strom, and R. Krejci (2013), Arctic aerosol life cycle: linking aerosol size distributions observed between 2000 and 2010 with air mass transport and precipitation at Zeppelin station, Ny-Alesund, Svalbard, *Atmospheric Chemistry and Physics*, *13*(7), 3643-3660, doi:10.5194/acp-13-3643-2013.

Udisti, R., et al. (2016), Sulfate source apportionment in the Ny-Alesund (Svalbard Islands) Arctic aerosol, *Rendiconti Lincei-Scienze Fisiche E Naturali*, *27*, 85-94, doi:10.1007/s12210-016-0517-7.

UNEP (2011), United Nations Environment Programme: Near-term Climate Protection and Clean Air Benefits: Actions for Controlling Short-Lived Climate Forcers, available at: http://www.unep.org/publications/ebooks/SLCF/ (last access: 29 August 2016), Nairobi, Kenya.

Wexler, A. S., and S. L. Clegg (2002), Atmospheric aerosol models for systems including the ions H+, NH4+, Na+, SO42-, NO3-,Cl-, Br-, and H2O, *Journal of Geophysical Research-Atmospheres*, *107*(D14), doi:10.1029/2001jd000451.

Wiedensohler, A., et al. (2012), Mobility particle size spectrometers: harmonization of technical standards and data structure to facilitate high quality long-term observations of atmospheric particle number size distributions, *Atmospheric Measurement Techniques*, *5*(3), 657-685, doi:10.5194/amt-5-657-2012.

786 Xu, J. W., et al. (2017), Source attribution of Arctic black carbon constrained by aircraft and surface
787 measurements, *Atmospheric Chemistry and Physics*, *17*(19), 11971-11989,
788 doi:10.5194/acp-17-11971-2017.
789 Zhao, C. F., and T. J. Garrett (2015), Effects of Arctic haze on surface cloud radiative forcing,
790 *Geophysical Research Letters*, *42*(2), 557-564, doi:10.1002/2014gl062015.